Exclusion of Gas Sparger Influence on Mass Transfer in Bubble Columns

W.-D. DECKWER and J. HALLENSLEBEN

Institut für Technische Chemie, Universität Hannover, Callinstr. 3, D-3000 Hannover 1, FRG

and

M. POPOVIC

Institut für Gärungsgewerbe und Biotechnologie, Seestr. 13, D-1000, Berlin 65, FRG

Gas phase CO_2 concentration profiles were measured in two sizes of bubble columns with different gas spargers and with the liquid phase (tap water) entrance or exit (cocurrent or countercurrent flow) at a certain height above the gas distributor. The region of high turbulence intensity near the sparger was locally separated from the region of high mass transfer rates in such columns. A modified back flow cell model was applied to describe the experimental data. The k_L-values obtained from fitting the profiles agreed for both columns and, in addition, did not differ for cocurrent and countercurrent flow. This is in remarkable contrast to previous findings[10,11]. The large influence of the gas sparger on the k_L-values even in tall bubble columns was thus demonstrated. It is thought that this may probably be one of the reasons why correlations for prediction of k_L differ so significantly.

On a mesuré les profils de concentration de $C0_2$ en phase gazeuse dans deux colonnes à bulles de dimensions différentes, en employant différents barboteurs à gaz et en s'assurant que l'entrée ou la sortie (selon l'écoulement est à co-courant ou à contre-courant) de la phase liquide (eau ordinaire) soit à une certaine hauteur au-dessus du distributeur de gaz. On a séparé localement la zone fortement turbulente proche du barboteur, de celle où les transferts de masse sont importants dans de telles colonnes; on a employé un modèle modifié de cellule à rétro-écoulement pour décrire les résultats expérimentaux. Les valeurs de k_L obtenues par "curve fitting" des profils ont concordé pour les deux colonnes et on a obtenu les mêmes valeurs, qu'il se soit agi d'un écoulement à co-courant ou à contre-courant. Cette constatation est en contradiction avec les résultats antérieurs[10,11]. On a ainsi démontré l'influence considérable exercée par le barboteur à gaz sur les valeurs de k_L, même dans des colonnes à bulles de grande hauteur; il y a lieu de croire qu'on trouve probablement là une des raisons pour lesquelles les corrélations servant à prévoir les valeurs de k_L diffèrent autant entre elles.

Numerous experimental studies on the interphase mass transfer in bubble columns and other gas/liquid reactors can be found in the literature. In part of these studies the parameters which may be of possible influence on gas/liquid mass transfer covered a considerable range. Despite the large amount of data one did not yet succeed in establishing reliable correlations which, for instance, predict the liquid side mass transfer coefficient with sufficient accuracy. Table 1 gives a summary of correlations proposed in the literature. The more frequently recommended relations are underlined. If one calculates Sherwood numbers on the basis of these proposals the predictions differ usually by several hundred percent even if one considers only the more recommended equations. Thus Sherwood numbers, for instance, calculated for oxygen transfer from bubbles are different by a factor of more than 5 as shown in Table 1. There are several reasons which cause that mass transfer coefficients scatter so broadly. Some major points appear to be the following ones:

(i) application of insufficient measuring techniques

(ii) evaluation on the basis of too simplified model assumptions.

It was shown[9-13] that the often carried out one-point measurements[6,12-17] do not give unambiguous results. Only additional measurements inside the equipment i.e. taking up the concentration profiles lead to sufficient information which, in addition, are to be evaluated by application of pertinent models in order to obtain reliable mass transfer data. This was already pointed out by Deckwer et al[18] who studied oxygen mass transfer at cocurrent flow in tall bubble columns.

In previous studies[10,11] the interphase mass transfer of CO_2 was investigated in bubble columns by measuring concentration profiles in both phases. The measured mass transfer rates were high as the applied CO_2 inlet concentrations were large (up to 80 percent) and the CO_2 solubility is rather large. It was therefore thought that in these studies hydrodynamic conditions could be simulated which are encountered in industrial applications of bubble columns as reactors. The evaluation of the measured concentration profiles was carried out on the basis of a rather sophisticated dispersion model which took into account very detailed knowledge of the locally dependent hydrodynamic properties determined experimentally. Unfortunately, it was not possible to match measured profiles and model predictions if a k_L-value was used which was assumed to be constant along the column. Figure 1 presents a typical result, i.e. a gas phase profile measured at cocurrent absorption in a 440 cm bubble column. This figure should actually be Fig. 9 in ref. [11]. It can be recognized from Figure 1 that the experimental outlet concentration is predicted by the model with good accuracy for a considerable range of k_L-values. But a satisfactory description of experimental profiles in the lower part of the column could not be achieved. Therefore increased k_L-values were applied in the region adjacent to the gas distributor ($0 \leqslant z \leqslant 0.05$). Thus an excellent description of the experimental data could be obtained. However, the k_L-values used to match the measured profiles did not only depend on the type of the gas sparger — which was found in oxygen mass transfer studies[7,9,18] too — but also on the operating conditions, i.e. absorption

TABLE 1

CORRELATIONS FOR LIQUID SIDE MASS TRANSFER COEFFICIENTS IN GAS/LIQUID DISPERSIONS

Author	Correlation	Sh^*_{calc}
Fröβling, 1938[1]	$Sh = 2 + 0.552\ Sc^{1/3}\ Re^{1/2}$	128
Ranz, Marshall, 1952,[2]	$Sh = 2 + 0.95\ Sc^{1/3}\ Re^{1/2}$	219
Calderbank, Moo-Young, 1961[3],	$Sh = 0.42\ Sc^{1/2}\ Gr^{1/3},\ d_B > 2.5$ mm	556
Hughmark, 1967[4]	$Sh = 2 + 0.0187 \left[Sc^{0.339} Re^{0.484} \left(\frac{d_s g^{1/3}}{D_L^{2/3}} \right)^{0.072} \right]^{1.61}$	272
Reuβ, 1970[5]	$Sh = 0.63\ Sc^{1/2}\ Re^{1/2} \left(\frac{1 - \epsilon_G}{1 - \epsilon_G^{1/3}} \right)^{1/2}$	519
Akita, Yoshida, 1974[7]	$Sh = 0.5\ Sc^{1/3} \left(\frac{g d_s^3}{\nu_L^2} \right)^{1/4} \left(\frac{g d_s^2 \rho_L}{\sigma} \right)^{3/8}$	88
Schügerl, et al., 1977[7]	$Sh = 0.15\ Sc^{1/2}\ Re^{3/4}$	517
Gestrich et al., 1976[8]	$Sh = \frac{d_s}{D_L} \left[2.23 \cdot 10^{-4} \left(\frac{\sigma^3 \rho}{\varrho \eta^4} \right)^{0.18} + 3.85 \cdot 10^{-3} (u_G^{0.65 + 0.0335 (H_o/D)} \cdot (H_o/D)^{-0.605} \right]$	244

*oxygen transfer in water at 20 °C

or desorption and cocurrent or countercurrent flow, respectively.

It can be argued that the increase of k_L at the column bottom may be caused by increased turbulence intensity due to the high energy dissipation at the gas distributor. On the other hand, it was reported in[11] that large frequency factors for bubble coalescence occur if the interphase mass transfer rates are high which is particularly the case near the gas sparger for cocurrent flow where the phases meet each other at first. One can expect that high rates of bubble coalescence lead to increased mass transfer. However, from the previous results it was not possible to discriminate which of these phenomena — energy dissipation or high coalescence rates due to large absorption — play the dominant role in raising the k_L-values. Therefore the present study was carried out at conditions where a possible influence of the gas distributor was excluded or reduced considerably, at least.

Experimental

Cocurrent and countercurrent absorption of CO_2 from air in water was studied in two bubble columns of different size. The columns were the same as those used in previous study[11] and some details of the experimental arrangement are given there. Table 2 summarizes some characteristic data of the two columns. To avoid formation of the gas/liquid dispersion and high mass transfer rates taking place at about the same position within the column, the liquid phase entered or left, respectively, the column at a a certain length above the gas sparger (see Table 2). Thus the formation of the gas/liquid dispersion and the region of high mass transfer rates were locally separated. The inlet gas velocities were varied from about 1 to 5 cm/s, thus operation in the

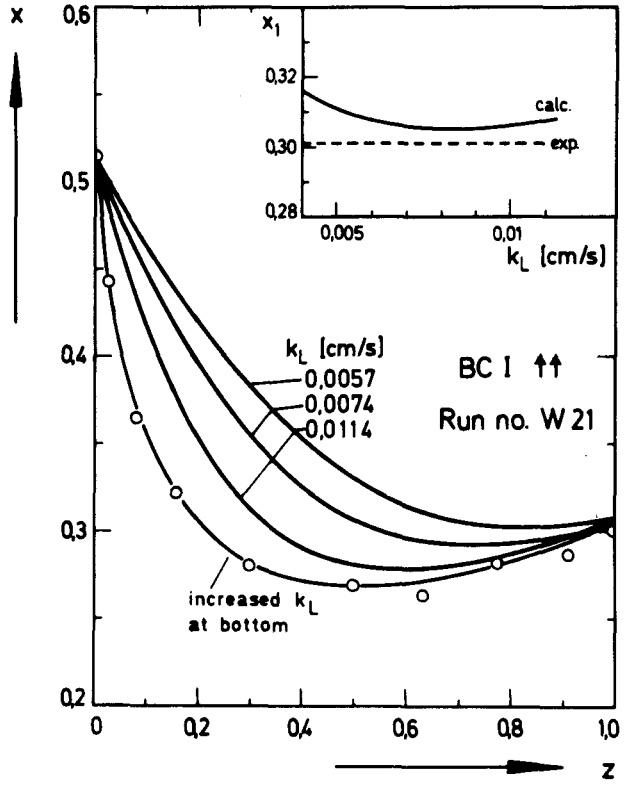

Figure 1 — Measured point values of CO_2 concentration in gas phase compared with computations using various k_L- values.

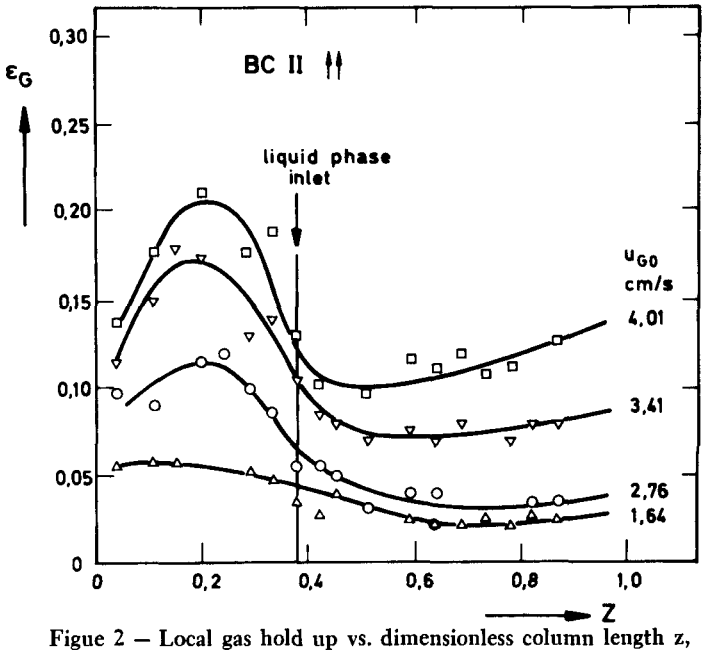

Figue 2 — Local gas hold up vs. dimensionless column length z, cocurrent flow.

TABLE 2

DETAILS OF USED BUBBLE COLUMNS

Bubble column	BC I	BC II
Length, cm	723	440
Diameter, cm	20	15
Gas distributor	cross with 56 holes, 1 mm ϕ	porous sintered plate (glass)
Liquid inlet/outlet above gas sparger, cm	218	165

pseudohomogeneous flow regime was guaranteed. The liquid flow rate was 3 m³/h throughout. Gas phase concentrations and local hold up values of the phases were determined along the column. The complete experimental arrangement and the applied measuring techniques are described in[11,19].

Gas hold up

Figure 2 presents some measured gas hold up profiles for cocurrent absorption runs in BC II. At that point where the liquid phase enters the column the gas hold up decreases considerably. This is caused by the special flow pattern and possibly also by the high absorption rates in that region of the column. It demonstrates indeed that hydrodynamic conditions are simulated which may be encountered in chemical reactors. For the evaluation of the measured gas phase profiles on the basis of a pertinent model it is necessary to take into account the local variations of ϵ_G and the specific interfacial area a. Therefore the course of ϵ_G is expressed by the following function:

$$\epsilon_G(z) = \bar{\epsilon}_G \varphi(z) \quad \ldots\ldots (1)$$

$$\varphi(z) = \sum_{i=1}^{3} b_i z^i \quad \ldots\ldots (2)$$

The b_i values are determined from the experimental data by a regression method. $\bar{\epsilon}_G$ in Equation (1) presents the integral or mean value of the gas holdup. In [11] it was concluded from a lot of experimental data that the average Sauter diameter of the bubbles in water is about 0.286 cm for the two columns used. This value was not only confirmed for different systems but also for different positions along the columns. No significant differences were found. Merely quite close to the gas sparger d_s is somewhat smaller. However, this causes an increase in interfacial area which is always less than 25 percent. It is therefore assumed that d_s is sufficiently constant over the column length. Applying a constant value of d_s = 0.286 cm the local interfacial area can be calculated by the relation:

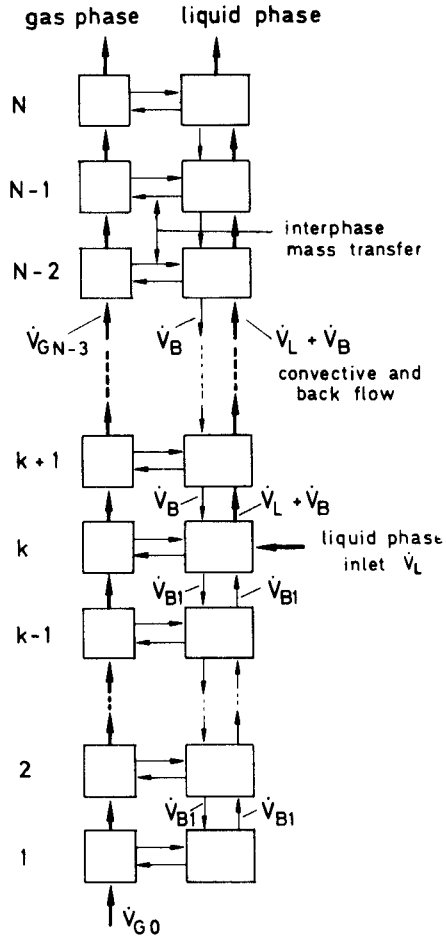

Figure 3 Schematic presentation of BFCM for cocurrent flow.

$$k_L = k_{L0}(1 + a e^{-b(j-k^2)})$$

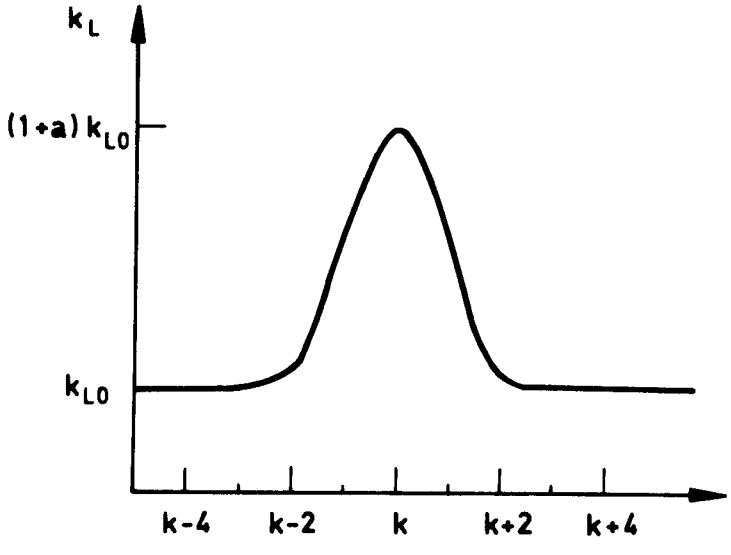

Figure 4 — Dependency of k_L on cell number applied in computations.

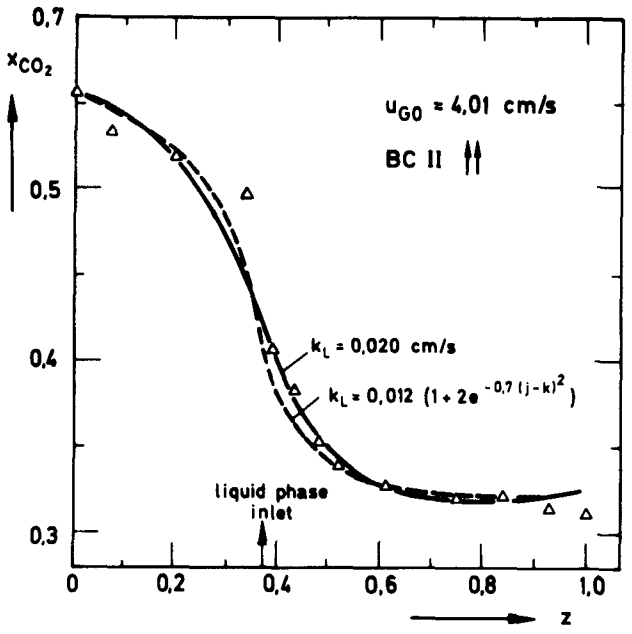

Figure 5 — Influence of a variable k_L on matching the measured data.

$$a(z) = 6\,\bar{\epsilon}_G\,\varphi(z)/d_S \quad \ldots\ldots (3)$$

This equation will be applied in the theoretical calculations which are carried out to describe the measured gas phase profiles.

Back flow cell model (BFCM)

Owing to the special arrangement of the liquid flow used in the present investigation a model description on the basis of the continuous dispersion model will be difficult. As the liquid phase separates in 2 regions with and without convective flow, respectively, and special boundary conditions have to be applied at the liquid inlet the numerical solution method used in [11] must be modified considerably. In addition, as was reported in [11,20], that the applied solution method did not converge for certain parameter combinations. It was assumed that these convergence difficulties are to be attributed to stiffness of the system of differential equations.

Therefore it was preferred to start from a lumped description of the bubble columns. Such a lumped version of the continuous dispersion model equations presents the two phase cell model with back flow (BFCM) for simulating the mixing. The BFCM was firstly applied to extractors and a comprehensive review on applications of the BFCM is given in [21]. The treatment on the basis of the BFCM can be extended to bubble column reactors if some modifications are introduced. Comprehensive numerical simulations with the continuous and the lumped model have shown that both models are equally suited to predict concentration profiles and conversions in bubble column reactors[22,23]. However, the BFCM has the advantage of larger flexibility to simulate easily more complex flow systems.

Figure 3 presents a schematic picture of modelling the cocurrent flow experiments of this study on the basis of the BFCM. It consists of two series of equal sized mixed cells. Mass transfer takes place between cells of the gas and liquid phase. In the liquid phase back flow and exchange flows are introduced to simulate axial dispersion. The mixing parameters of

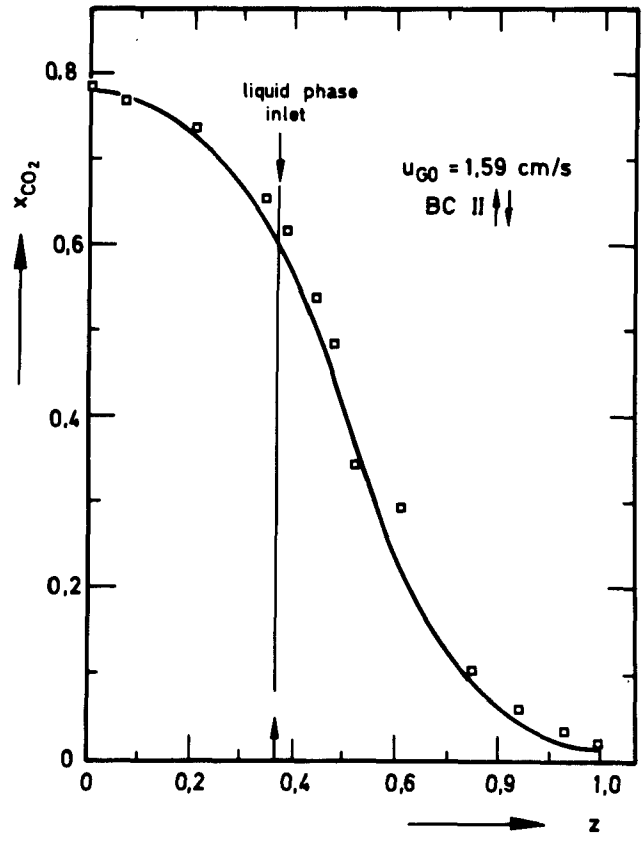

Figure 6 — Experimental and computed profiles, BC II, countercurrent flow.

the BFCM and the dispersion model are interrelated by the well-known relation[21]:

$$\gamma = N/Pe_L - 0.5 \quad \ldots\ldots (4)$$

Here N is the entire cell number used in the BFCM and γ represents the ratio of black flow, to convective flow. It can be shown that for the region below the liquid phase inlet or outlet where no overall convective flow occurs Equation (4) reduces to

$$\gamma = N/Pe_L \quad \ldots\ldots (5)$$

Equations (4) and (5) are not quite correct for the present experiments as they refer to conditions under which the phase hold ups are constant. As in this study the variation of ϵ_L along the column is, however, small application of Equation (4) and (5) will suffice. The complete equation for relating the mixing parameters of both models is given in [23]. The Peclet number of the liquid phase is calculated from a correlation for the dispersion coefficient which was presented in [18] and recently recommended in a review paper[24]. Due to the small diameters of the columns used gas phase dispersion can be neglected. With $N = 20$ one obtains $Pe_G \approx 40$, hence the plug flow assumption is fulfilled with sufficient accuracy. The further essential assumptions to describe our measurements with the BFCM are as follows:

(1) steady state isothermal operation
(2) Henry's law applies
(3) O_2 and N_2 are inerts
(4) gas hold up and interfacial area vary with z
(5) owing to the hydrostatic head the pressure varies linearly with z
(6) gas velocity is variable
(7) neglect of reaction of CO_2 with water

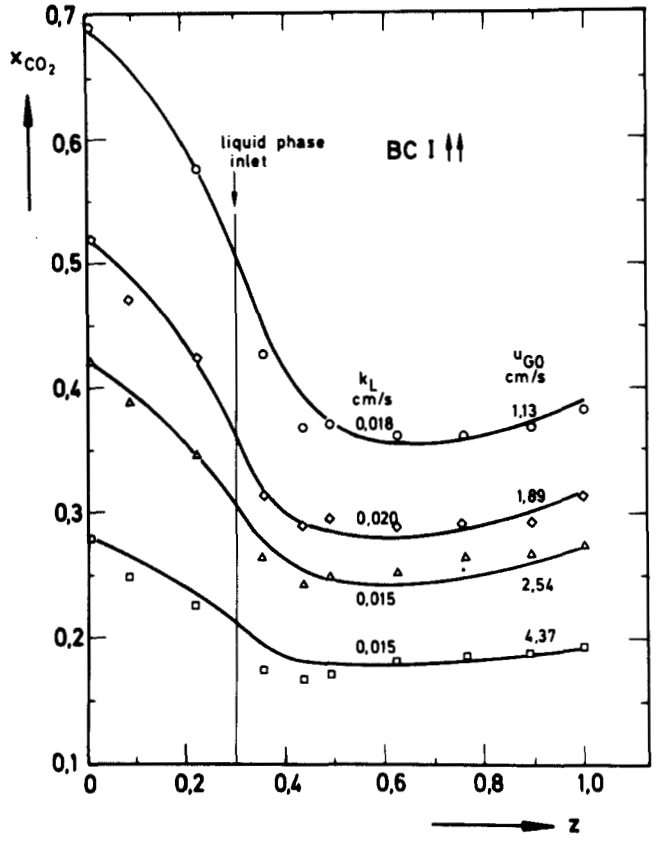

Figure 7 — Computed and measured profiles in BC I, co-current flow.

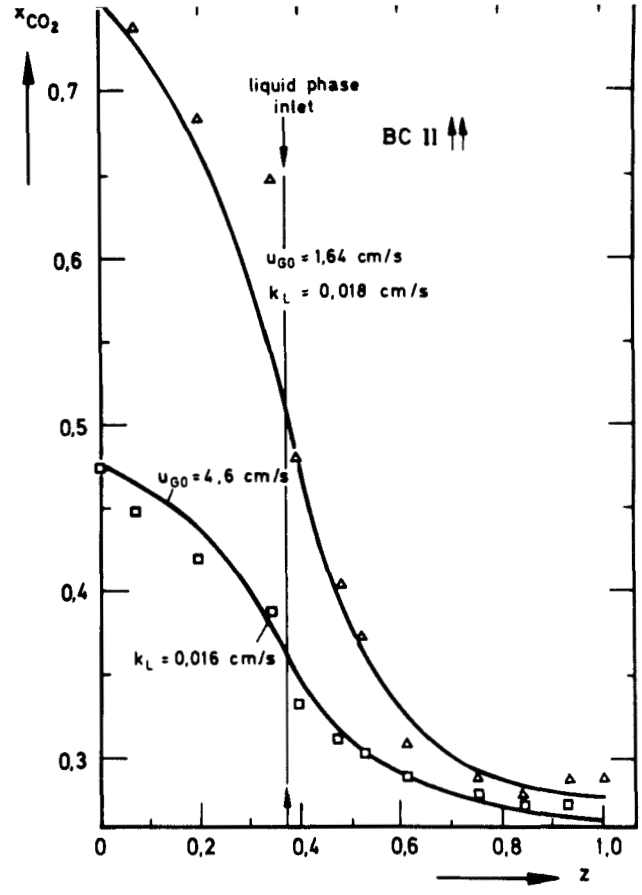

Figure 8 — Computed and measured profiles in BC II, co-current flow.

The governing balance equations of the BFCM are derived in a straight forward manner. For the CO_2 in the gas phase the balance around cell j yields:

$$\dot{V}_{Gj-1}c_{Gj-1} - \dot{V}_{Gj}c_{Gj} - k_{Lj}(A/N)(c_j^* - c_j) = 0 \quad (6)$$

Introducing

$$c_{Gj} = P_j x_j/RT \quad (7)$$

$$\bar{u}_{Gj} = \dot{V}_{Gj}/\dot{V}_{Go} \quad (8)$$

$$c_j^* = P_j x_j/H \quad (9)$$

$$A = a(z)QL = 6\bar{\epsilon}_G\,\varphi(z)QL/d_S \quad (10)$$

one obtains:

$$\bar{u}_{Gj-1}P_{j-1}x_{j-1} - \bar{u}_{Gj}P_j x_j - [6k_{Lj}\bar{\epsilon}_G\varphi(z)RTL/(u_{Go}HNd_s)] (P_j x_j - c_j H) = 0 \quad (11)$$

The pressure profiles in the continuous model is given by

$$P(z) = P_T + \rho g\bar{\epsilon}_L(1 - z)L \quad (12)$$

where P_T is the pressure at column top. The axial coordinate z and the cell number j of the BFCM are related by

$$z = (j - 0.5)/N \quad (13)$$

Using this relation one obtains from Equation (12)

$$P_j = P_o(1 + \alpha j) \quad (14)$$

with

$$P_o = P_T + \rho g\bar{\epsilon}_L L(N + 0.5)/N \quad (15)$$

and

$$\alpha = -\rho\, g\bar{\epsilon}_L L/(NP_o) \quad (16)$$

The gas phase balance of CO_2 becomes therefore:

$$[1 + \alpha(j - 1)]\, x_{j-1}\bar{u}_{Gj-1} - [1 + \alpha j]\, x_j\bar{u}_{Gj} - St_{Gj}[(1 + \alpha j) x_j - c_j H/P_o] = 0 \quad (17)$$

with the gas phase Stanton number of cell j:

$$St_{Gj} = (k_{Lj}/N)(6\bar{\epsilon}_G\varphi_j/d_S)(L/u_{Go})(RT/H) \quad (18)$$

As the change of the gas flow rate caused by absorption and pressure decrease has to be taken into account the gas velocity is an additional variable which requires consideration of the entire gas phase balance. This is obtained similar to the gas phase component balance:

$$[1 + \alpha(j - 1)]\,\bar{u}_{Gj-1} - (1 + \alpha j)\,\bar{u}_{Gj} - St_{Gj}[(1 + \alpha j) x_j - c_j H/P_o] = 0 \quad (19)$$

In equations (18) and (19) the cell number runs from 1 to N. The zero-indexed variables are

$$x_o = x_{inlet}$$

$$\bar{u}_{Go} = 1.$$

For deriving the liquid phase balance equations one has to distinguish for cocurrent and countercurrent flow. Considering cell j with $k < j < N$ and cocurrent flow ($\uparrow\uparrow$) one obtains from figure 3

$$(\dot{V}_L + \dot{V}_{BL})\, c_{j-1} - (\dot{V}_L + 2\dot{V}_{BL})\, c_j + \dot{V}_{BL}\, c_{j+1} + k_{Lj}(A/N)(c_j^* - c_j) = 0 \quad (20)$$

Introduction of the dimensionless back flow ratio

$$\gamma = \dot{V}_{BL}/\dot{V}_L \quad (21)$$

and the liquid phase Stanton numbers:

$$St_{Lj} = (k_{Lj}/N)(6\bar{\epsilon}_G\varphi_j/N)(L/u_L)/d_s \quad (22)$$

$$St'_{Lj} = St_{Lj}\, P_o(1 + \alpha j)/H \quad (23)$$

leads to:

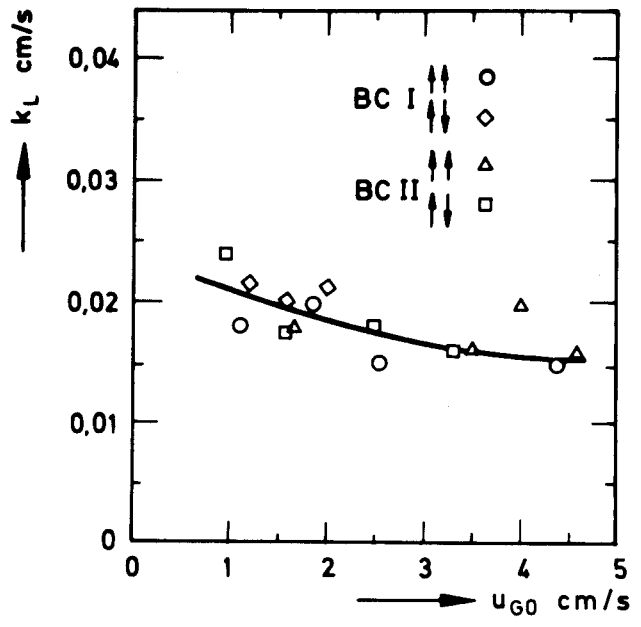

Figure 9 – Mass transfer k_L from fitting measured profiles.

$$(1 + \gamma_1)\, c_{j-1} - (1 + 2\gamma + St_{Lj})\, c_j + \gamma c_{j+1} + St'_{Lj}\, x_j = 0 \quad (24)$$

The other balance equations are derived similarly. The complete set of the liquid phase equations for cocurrent and countercurrent flow is as follows:

$$j = 1: -(\gamma_1 + St_L)\, c_1 + \gamma_1 c_2 + St'_{L1} x_1 = 0 \quad (25)$$

$$1 < j < k: \gamma_1 c_{j-1} - (2\gamma_1 + St_{Lj})\, c_j + \gamma_1 c_{j+1} + St'_{Lj} x_j = 0 \quad (26)$$

$$j = k: \gamma_1 c_{k-1} - (1 + \gamma_1 + \gamma + St_{Lj})\, c_k + (a_o + \gamma)\, c_{k+1} + St'_{Lj} x_k = 0 \quad (27)$$

$$\uparrow\uparrow: a_o = c_{inlet}/c_{k+1} \qquad \uparrow\downarrow: a_o = 1$$

$$k < j < N: (a_1 + \gamma) c_{j-1} - (1 + 2\gamma + St_{Lj})\, c_j + (a_2 + \gamma)\, c_{j-1} + St'_{Lj} x_j = 0 \quad (28)$$

$$\uparrow\uparrow: a_1 = 1,\ a_2 = 0 \qquad \uparrow\downarrow: a_1 = 0,\ a_2 = 1$$

$$j = N: (a_3 + \gamma)\, c_{N-1} - (1 + \gamma + St_{LN})\, c_N + St'_{LN} x_N = 0 \quad (29)$$

$$\uparrow\uparrow: a_3 = 1 \qquad \uparrow\downarrow: a_3 = c_{inlet}/c_{N-1}$$

The inlet concentration of CO_2 was always zero in the present measurements. The back flow ratio in the lower part of the column without convective flow is denoted by γ_1 and is calculated from Equation (5) while γ is obtained by Equation (4).

From our previous investigations[11] it appeared possible that a k_L profile must be introduced to match the theoretical predictions to measured profiles. Therefore the following dependency of k_L on j was built into the model equations:

$$k_{Lj} = k_{Lo}[1 + a \exp(-b(j - i)^2)] \quad (30)$$

This function (discrete Gaussian) yields particularly increased k_L-values if $j = i$ as can be seen from Figure 4 where Equation (30) is plotted for $i = k$. One can suspect from our recent results that increased k_L values occur either near the sparger ($i = 1$) caused by the high energy dissipation or at the liquid phase inlet (for cocurrent flow) due to the large negative overall frequency factors[11] which indicates high coalescence rates caused by appreciable absorption.

The BFCM leads to a set of 3 N algebraic equations which are needed to determine the 3 N unknowns. N was set to 20, thus 60 algebraic equations were to be solved.

As the CO_2 gas phase balance equations are nonlinear an iterative solution procedure was necessary. Two methods were used:

(1) Newton's method: Here the equations were linearized and then solved by Gauss elimination. Usually no more than 3 to 4 iterations were needed.

(2) Successive overrelaxation (SOR): This iterative method takes advantage of the fact that matrix of the coefficients consists mainly of zeros. Linearization of the equations is not needed.

Though the SOR method requires more iterations, of course, the computation times required for both solution methods are comparable for the present problem.

Description of measured gas phase profiles

For the evaluation of the measured gas phase profiles only those runs were used for which the overall CO_2 balance agreed within 3%. The entire number of runs was 16, and the overall balances were fulfilled for 15 runs within

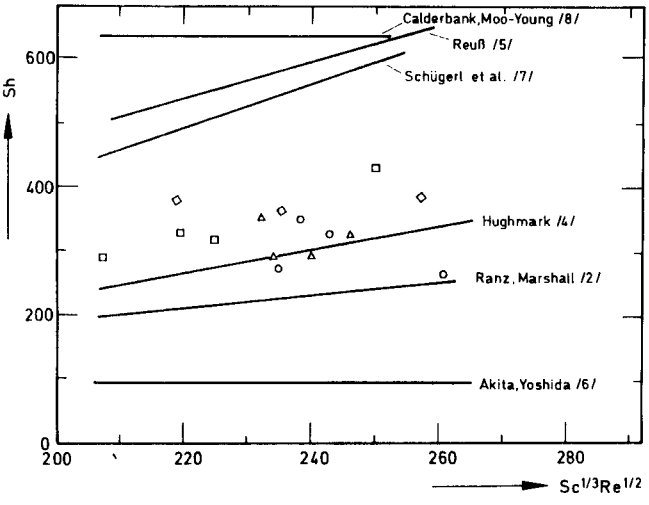

Figure 10 – Comparison of experimental Sherwood number with predictions from correlations.

the given limit. In the theoretical computations all parameters involved in the model equations are known except the k_L-value which is varied in the calculations. In order to fit the experimental results by predictions of the BFCM it was therefore necessary first of all to clarify whether a k_L-value which is constant along the column or a k_L-profile like that presented by Equation (30) has to be applied. Therefore numerous calculations were carried out with different values of a, b and i in Equation (30). A typical result for a cocurrent run is presented in Figure 5. Here the full drawn curve is calculated with a constant k_L of 0.02 cm/s whereas the dotted curve is obtained from a k_L-profile as indicated in that figure. This profile yields a threefold increase of k_L at the point where the liquid phase is fed into the column ($j = 8$, $z = 0.378$). The computations shown in figure 5 reveal that application of increased k_L-values at the liquid phase inlet does not significantly improve the description of the measured points. In both cases the agreement with the model predictions is fairly good. The same result was obtained for the other cocurrent and countercurrent runs in the two bubble columns. Hence one has to conclude that contrary to our previous findings there is no need to apply locally dependent k_L-values for matching the measured gas phase profiles. This is demonstrated in the following figures where k_L values being constant over the entire column length lead to a good agreement between measurements and model calculations. Figure 6 shows a x_{CO_2} profile for countercurrent flow in BC II. The mole fraction of CO_2 drops down from 0.78 to almost zero at the outlet. Though there seem to be some systematic deviations between the measured data and the predicted values it is believed that the achievable description is fair. For this case, too, consideration of a k_L profile does not improve the fitting of the experimental data to such an extent that introduction of a k_L-profile would be justified. Further measured results and computed curves for cocurrent runs are presented in Figures 7 and 8. Here the description on the basis of BFCM by using a constant k_L can be denoted as rather good.

Liquid side mass transfer coefficients k_L

The k_L-data obtained from fitting the measured point values are plotted *vs* the inlet gas velocity in Figure 9. Though the data show some scatter, there are no noticeable differences between the two columns. Also no dependency on the direction of liquid flow ($\uparrow\uparrow$ or $\uparrow\downarrow$) is observed. The Sherwood numbers calculated from the k_L-values are plotted in Figure 10 and compared with several empirical correlations. As can be expected most correlations fail completely, only the relation proposed by Hughmark gives a reasonable approximation though the scatter is considerable too.

Interpretation of results and conclusions

In this study where the liquid inlet or outlet, respectively, were separated from the gas distributor the experimental data can be fitted with a k_L-value being constant along the column. With respect to the findings reported in [10,11] where increased k_L-values in the vicinity of the gas sparger had to be introduced for fitting the measurements this observation presents an important result since it reveals that the increase in k_L is exclusively caused by the high turbulence intensity near the sparger and not an effect due to the high coalescence rates caused by strong absorption as could be suspected from the negative overall frequency factors reported in[11]. It is also important to emphasize that the k_L-values shown in Figure 9 do not differ for cocurrent and countercurrent flow. Hence the splitting of the k_L-values for different operating conditions found in [11] cannot be confirmed by the present results. Obviously the splitting of k_L-data for the main part of the columns appears to be merely a result of the need to apply increased k_L-values caused by the high turbulence intensity at the gas distributor.

In addition it should be pointed out that the k_L-data of both columns do not differ though they are equipped with different gas spargers. This result is rather surprising as it was not only shown in [10,11] but also in oxygen mass transfer studies in tall bubble columns[7,9,18] that sintered plates yield appreciably higher k_L-values than perforated plates with bores larger than 0.5 mm. It can be suspected that the effect of the sparger is one of the reasons that the numerous correlations proposed in the literature (s. Table 1 and Figure 10) lead to so broadly different predictions as none of them considers explicitly gas sparger properties.

It is commonly assumed to regard the influence of the gas sparger as a typical inlet effect which becomes negligible at larger gas velocities and high columns, respectively. Several studies on physical mass transfer[7,9,11,18] indicate that this conclusion is not permitted if the liquid flow is arranged in the normal manner, i.e. the liquid enters or leaves the columns at the gas distributor. The results of Voigt and Schügerl[25] particularly show that in short columns the k_La-value significantly depends on liquid height. It was also found that liquid phase concentration profiles of oxygen measured in bubble column fermenters can only be explained by assuming increased k_L-values for O_2 at the gas sparger[26,27] This dependency of k_L may particularly exert a distinct influence on the overall conversion if the sink term in the gas phase balance depends on k_L as is the case for the slow and instantaneous regime of absorption theory.

The measurements of this study were evaluated by use of the BFCM. An excellent description of the gas phase profiles could be achieved. Convergence difficulties were not observed. This indicates that the BFCM is a very efficient and convenient method to describe gas/liquid flow contactors. In particular, the BFCM exhibits a large flexibility and adaptability to model different flow patterns at various conditions.

Acknowledgment

The authors gratefully acknowledge financial support from Deutsche Forschungsgemeinschaft and Stiftung Volkswagenwerk.

Symbols

A = interfacial area
a = specific interfacial area
b_i = coefficients in equation (2)
c = liquid phase concentration
c^* = saturation value of liquid phase concentration, see equation (9)
c_G = gas phase concentration
D_L = diffusion coefficient in liquid phase
d_s = Sauter diameter
Gr = Grashof number
g = gravitational acceleration
H = Henry's constant
H_o = liquid height in column
j = cell number
k_L = liquid side mass transfer coefficient
L = height of gas/liquid dispersion
N = entire cell number
P = pressure
P_T = pressure at column top
Pe_L = liquid phase Peclet number
Q = cross sectional area of column
R = gas constant

Re = Reynolds number
Sc = Schmidt number
Sh = Sherwood number
St_G = gas phase Stanton number, see equation (18)
St, St'_L = liquid phase Stanton numbers, see Equations (22) and (23)
T = temperature
u_G = linear gas velocity
$\bar{u}_G$ = dimensionless gas velocity, see Equation (8)
$\dot{V}_G$ = gas flow rate
$\dot{V}_L$ = liquid flow rate
$\dot{V}_{BL}$ = back flow in liquid phase
x = mole fraction in gas phase
z = dimensionless axial coordinate

α = pressure ratio, def. by Equation (16)
γ = back flow ratio, see Equation (21)
ϵ_G = relative gas hold up
$\bar{\epsilon}_G$ = mean relative gas hold up
η = dynamic viscosity
ν = kinematic viscosity
ρ = density (of liquid phase)
σ = surface tension
φ = function defined by Equation (2)

Indices

$_0$ = column inlet
$_G$ = gas phase
$_L$ = liquid phase
$_j$ = cell number

References

(1) Fröβing, N., Gerlands Beitr. Geophys. **32**, 170 (1938).
(2) Ranz, W. E. and Marshall, W. R., Chem. Eng. Prog. **48**, 141 (1952).
(3) Calderbank, P. H. and Moo-Young, M. B., Chem. Eng. Sci. **16**, 39 (1961).
(4) Hughmark, G. A., Ind. Eng. Chem. Process Des. Dev. **6**, 219 (1967).
(5) Reuβ, M., Dr. Ing. Thesis, TU Berlin (1970).
(6) Akita, K. and Yoshida, F., Ind. Eng. Chem. Process Des. Dev. **13**, 84 (1974).
(7) Schügerl, K., Oels, U. and Lücke, J., Adv. Biochem. Bioeng. **7**, 1 (1977).
(8) Gestrich, W., Eisenwein, H. and Krauss, W., Chem. Ing. Tech. **48**, 399 (1976).
(9) Burckhart, R. and Deckwer, W.-D., Verfahrenstechnik **10**, 429 (1976).
(10) Deckwer, W.-D., Adler, I. and Zaidi, A., ACS Symp. Series No. 65 (1978) Chem. React. Eng. - Houston, ed. by V. W. Weekman, Jr. and D. Luss.
(11) Deckwer, W.-D., Adler, I. and Zaidi, A., Can. J. Chem. Eng. **56** 43 (1978).
(12) Hsu, K. H., Erickson, L. E. and Fan, L. T., Biotechnol. Bioeng. **19**, 247 (1977).
(13) McLean, G. T., Erickson, L. E., Hsu, K. H. and Fan, L. T., Biotechnol. Bioeng. 19, 493 (1977).
(14) Eckenfelder, W. W. and Barnhart, E. L., AIChE-J. **7**, 631 (1961).
(15) Voyer, R. D. and Miller, A. I., Can. J. Chem. Eng. **46**, 335 (1968).
(16) Chen, B. H. and Vallabh, R., Ind. Eng. Chem. Process Des. Dev. **9**, 121 (1970).
(17) Fan, L. T., Hsu, H. H. and Wang, K. B., J. Chem. Eng Data **20**, 26 (1975).
(18) Deckwer, W.-D., Burckhart, R. and Zoll, G., Chem. Eng. Sci. **29**, 2177 (1974).
(19) Deckwer, W.-D., Zaidi A. and Adler, I., Chem.-Ing.-Tech. 48, 1075 (1976), **49**, 507 (1977).
(20) Deckwer, W.-D., Chem. Eng. Sci. **31**, 309 (1976).
(21) Mecklenburgh, J. C. and Hartland, S., The Theory of Backmixing, Wiley, London (1975).
(22) Popovic, M., Dr. Ing. thesis, TU Berlin (1976).
(23) Popovic, M. and Deckwer, W.-D., paper C26 presented at Congrès International: "Contribution des Calculateurs électroniques au Développement du Génie Chimique et de la Chimie Industrielle", Paris (1978).
(24) Shah, Y. T., Stiegel, G. J. and Sharma, M. M., AIChE J. **24**, 369 (1978).
(25) Voigt, J. and Schügerl, K., Chem. Eng. Sci. **34**, 1221 (1979).
(26) Buchholz, H., Dr. thesis, Hanover Univ. (1979).
(27) Buchholz, H., Luttman, K., Zakrzewski, W. and Shügerl, K., Chem. Eng. Sci. **35**, 111 (1980), ISCRE 6, Nice, March 1980.

Manuscript received March 6, 1979; accepted for publication October 24, 1979.

★ ★ ★